Influence of the nature and environment of manganese in Mn-BEA zeolites on NO conversion in selective catalytic reduction with ammonia

Rafal Baran, L. Valentin, J.-M. Krafft, T. Grzybek, P. Glatzel, Stanislaw Dzwigaj

▶ **To cite this version:**

Rafal Baran, L. Valentin, J.-M. Krafft, T. Grzybek, P. Glatzel, et al.. Influence of the nature and environment of manganese in Mn-BEA zeolites on NO conversion in selective catalytic reduction with ammonia. Physical Chemistry Chemical Physics, 2017, 176 (1), pp.229-233. 10.1039/C7CP02096A . hal-01527245

HAL Id: hal-01527245

https://hal.sorbonne-universite.fr/hal-01527245v1

Submitted on 24 May 2017

HAL is a multi-disciplinary open access archive for the deposit and dissemination of scientific research documents, whether they are published or not. The documents may come from teaching and research institutions in France or abroad, or from public or private research centers.

L'archive ouverte pluridisciplinaire **HAL**, est destinée au dépôt et à la diffusion de documents scientifiques de niveau recherche, publiés ou non, émanant des établissements d'enseignement et de recherche français ou étrangers, des laboratoires publics ou privés.

PAPER

Influence of nature and environment of manganese in Mn-BEA zeolite on NO conversion in selective catalytic reduction with ammonia

R. Baran,[a,b,*] L. Valentin,[c] J.-M. Krafft,[c] T. Grzybek,[b] P. Glatzel[a] and S. Dzwigaj[c,*]

Manganese-containing BEA zeolites, Mn_xSiBEA (x = 1–4 wt %) and $Mn_{(I.E.)}AlBEA$, were prepared by a two-step postsynthesis method and a conventional wet ion-exchange, respectively, and applied as catalysts in the selective catalytic reduction of NO with ammonia (NH_3-SCR). The physicochemical analysis of zeolite properties by the high-energy-resolution fluorescence-detected XANES (HERFD-XANES) and X-ray emission spectroscopy (XES) uncovered that the coordination, geometry and oxidation state of Mn species are strongly related to the preparation method. Additionally, the study of catalysts acidity by FTIR spectroscopy with CO and pyridine probe molecules provided important insight into the number and type of acidic centres present on catalyst surface. The catalytic results revealed that NO conversion depended on the state and content of Mn. The zeolites obtained with the two-step postsynthesis method and with low Mn content were very active at medium temperature range (NO conversion ~100 %) with simultaneous high selectivity to N_2 due to the presence of isolated, framework Mn(III) and Mn(II) species. The N_2O formation was especially high for catalysts containing extra-framework polynuclear Mn species and negligible in the case of $Mn_{(I.E.)}AlBEA$ containing predominantly isolated, extra-framework Mn(II) species.

Introduction

The emission of nitrogen oxides (NO, NO_2 and N_2O) to the atmosphere has severe impact on the environment that can be mitigated by catalytic reduction of NO_x ($DeNO_x$). Despite numerous studies fundamental questions concerning the catalytic mechanism, intermediate complexes and site products formation remain unanswered[1–5]. One of the major challenge in $DeNO_x$ processes is to find catalysts that will allow effective conversion of NO_x to dinitrogen at low temperature in diesel systems or in SCR unit at tail-end configuration for coal fired boilers in order of limit the costs of exhaust preheating or reheating. The current solutions do not fulfil all economic and environmental requirements thus some improvements should be implemented.

Among the proposed new catalysts are manganese containing materials because of their high reactivity already below 425 K[6–9]. The literature data shows that advantageous catalysts in SCR of NO at low temperature are manganese oxides supported on TiO_2[10,11] and Al-SBA-15[12] as well as Mn-containing activated carbons[13]. However, their stability and/or selectivity to the desired products were not beneficial over 575 K, the use of catalysts in a wider temperature range is crucial for automotive NH_3-SCR system. The main obstacles were sintering of the active material and high N_2O yield. In contrast, Cu-promoted zeolites, for example, were found to be less prone to deactivation and highly selective to N_2 but not enough effective during the initial phase of operation when the car engine and catalyst are cold[14,15]. The development of catalyst preparation methods that allow precisely control of Mn speciation may improve NO_x mitigation efficiency.

In this work we studied properties of MnSiBEA and $Mn_{(I.E)}AlBEA$ catalysts obtained from parent BEA zeolite by a two-step postsynthesis method developed by Dzwigaj et al.[16,17] and by the conventional wet ion-exchange, respectively. The MnSiBEA prepared by novel postsynthesis method, composed of dealumination and impregnation steps, contains Mn species incorporated into the framework positions. Conversely, in $Mn_{(I.E)}AlBEA$ Mn centers are located in the extra-framework positions inside the zeolite cavities. Our comprehensive investigation unraveled various physicochemical properties of Mn species and their clear differences in catalytic activity in SCR of NO with ammonia.

Experimental

Materials

Manganese-containing BEA zeolites were prepared from parent TEABEA zeolite by a two-step postsynthesis method

[a] ESRF – The European Synchrotron, 71 Avenue des Martyrs, 38000 Grenoble, France.
[b] AGH University of Science and Technology al. A. Mickiewicza 30, 30-059 Krakow, Poland.
[c] Sorbonne Universités, UPMC Univ Paris 06, CNRS, UMR 7197, Laboratoire de Réactivité de Surface, F-75005, Paris, France.
*Corresponding authors: rafal.baran@esrf.fr; stanislaw.dzwigaj@upmc.fr
Electronic Supplementary Information (ESI) available

($Mn_{1.0}$SiBEA, $Mn_{2.0}$SiBEA and $Mn_{4.0}$SiBEA) and a conventional ion-exchange procedure ($Mn_{(I.E.)}$AlBEA) using SiBEA and HAlBEA as the supports. The preparation of the supports was described in our earlier work[18]. The $Mn_{1.0}$SiBEA, $Mn_{2.0}$SiBEA and $Mn_{4.0}$SiBEA were prepared by impregnation of 2 g of SiBEA with $Mn(NO_3)_2$ solutions with appropriate concentration of Mn. Firstly, the suspensions were stirred for 24 h at 298 K in excess solvent using 200 mL of the precursor solutions. Then, the suspensions were stirred in evaporator under vacuum of a water pump in air at 353 K for 2 h until water was evaporated. The $Mn_{(I.E.)}$AlBEA was prepared by stirring for 3 hours at 333 K the suspension of 2 g of HAlBEA and 200 mL of manganese(II) nitrate solution (C = 0.01 mol L^{-1}). Then the suspension was filtered and the obtained solid was washed with distilled water and dried at 363 K overnight. This procedure was repeated twice. The obtained Mn loading was 1.9 wt %.

All the samples were calcined in air (100 K h^{-1}) at 773 K for 3 h under static conditions and labeled as C-$Mn_{1.0}$SiBEA, C-$Mn_{2.0}$SiBEA, C-$Mn_{4.0}$SiBEA and C-$Mn_{(I.E.)}$AlBEA, where C- stands for calcined and index next to Mn symbol indicates its content.

Techniques

X-ray fluorescence chemical analysis was performed at room temperature on SPECTRO X-LabPro apparatus.

The XRD experiments were carried out on a PANalytical Empyrean diffractometer equipped with the Cu Kα radiation (λ = 154.05 pm) in the 2θ range of 5 – 90°. High-temperature XRD measurements were carried out using the same diffractometer equipped with an Anton Paar HT 1200N oven-chamber. The measurements were done in the air at 298 – 1173 K temperature range.

Diffuse reflectance UV−vis spectra were recorded in ambient atmosphere on a Cary 5000 Varian instrument using polytetrafluoroethylene as reference.

X-ray photoelectron spectroscopy (XPS) measurements were carried out using an Omicron (ESCA+) spectrometer and an Al Kα (hv =1486.6 eV) source. The X-ray source was equipped with a flood gun. The area of the analyzed sample was ca. 3 mm^2. The powder samples were prepared for measurements by pressing them on an indium foil. The binding energy (BE) scale was calibrated to the Si 1s peak at 103.3 eV. Zeolite samples were outgassed at room temperature to 10^{-7} Pa. All spectra were fitted with a Voigt function (a 70/30 composition of Gaussian and Lorentzian functions) in the CasaXPS software in order to determine the number of components under each XPS peak.

The acidic properties of Mn-containing zeolites were determined by pyridine and CO sorption combined with infrared spectroscopy as described in our previous work[19,20].

The XAS and XES experiments were carried out at beamline ID26 of the European Synchrotron Radiation Facility (ESRF) in Grenoble, France. The data were recorded on the pellets containing 5 wt % of the sample diluted in the cellulose. The incident energy was tuned through the Mn K edge by a pair of cryogenically-cooled Si(111) monochromator crystals. A Fe foil was used to calibrate the energy by setting the first inflection point of the Fe K edge to 7112 eV. The XES spectra were collected at incident energy of 6700 eV with a X-ray emission spectrometer equipped with a set of four spherically bent Ge(333) and Ge(440) crystals for Mn Kα and Kβ lines, respectively, and detected with an avalanche photodiode. The analyzer crystals were arranged in vertical Rowland geometry. The Mn Kα XES spectra were fitted with two Lorentzian functions to determine the full width at half maximum (FWHM) of the $K\alpha_1$ line. High-energy resolution fluorescence detected x-ray absorption near edge structure (HERFD-XANES) spectra were recorded for all zeolite samples at the maximum of the Mn $K\alpha_1$ line. The incident total flux was 10^{13} photons s^{-1}. A background subtraction was applied to the Mn Kβ valence-to-core X-ray emission spectra (VTC-XES) using the procedure proposed by Gallo and Glatzel[21] in order to remove the contribution of the 3p to 1s (Kβ) core-to-core (CTC) main line tail.

The tests of the catalyst activity in selective catalytic reduction (SCR) of NO with ammonia were performed in a fixed bed reactor. The composition of the reaction gas was: 1000 ppm NO, 1000 ppm NH_3, 3.5 vol. % O_2 and He as balance. The gas mixture was provided with calibrated electronic mass flow controllers (BETA-ERG). The total gas flow was 0.1 L min^{-1} and the catalyst mass was 0.2 g. The concentrations of NO and N_2O were analyzed by NDIR detectors (ABB 2020 AO series). Prior to the reaction the catalyst bed was activated in 3.5 % O_2/He flow (0.1 L min^{-1}) in the temperature range of 298–798 K with a linear heating rate of 2 K min^{-1} and then for 1 h at 798 K. The standard test was carried out over 1 h at 573–773 K with increasing reaction temperature every 50 K interval. The NO conversion was calculated from the measured concentration of nitrogen oxide. The N_2 selectivity was calculated based on following formula:

$$N_2\ selectivity\ (\%) = \frac{([NO]_{in} - [NO]_{out}) - [N_2O]_{out}}{[NO]_{in} - [NO]_{out}} \times 100$$

Results and discussion

Stability of the Mn-BEA catalysts

In our previous work, we have shown by XRD that Mn ions were introduced into the zeolite SiBEA matrix forming isolated, mononuclear Mn(II) and Mn(III) species[22]. In this work, we studied the zeolite durability by means of in-situ XRD during calcination at elevated temperature and in air atmosphere. The experiments were carried out between 298 – 1173 K. The temperature was gradually raised 100 K per step with 2 K min^{-1} ramp rate in order to follow the possible changes in the zeolite structure. The registered XRD profiles for $Mn_{(I.E.)}$AlBEA, $Mn_{1.0}$SiBEA and $Mn_{4.0}$SiBEA are shown in Figure 1. In the case of $Mn_{(I.E.)}$AlBEA, we observed an increase in the intensity of the main diffraction reflection (d_{302}) at around 22.5° with increase of the temperature from 298 to 773 K (without significant shift of the diffraction angle). In contrast, with further increase of the temperature the position of the main diffraction peak was

displaced to higher values of the 2θ angle (to 22.75° at 1173 K) with simultaneous decrease of its intensity. These observations suggest that above 773 K the process of thermal dealumination could occur with simultaneous modification of

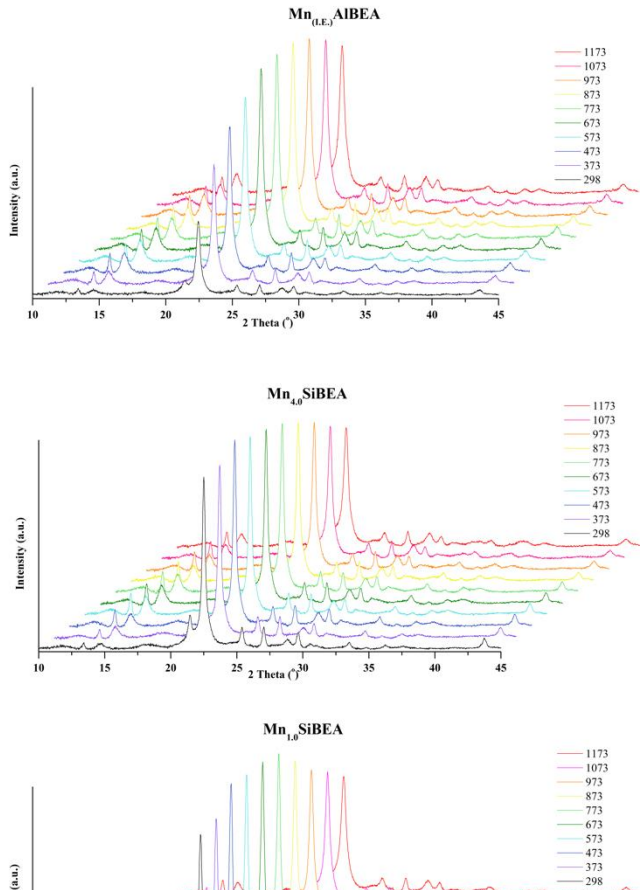

Figure 1 Evolution of XRD patterns of $Mn_{(I.E.)}AlBEA$, $Mn_{1.0}SiBEA$ and $Mn_{4.0}SiBEA$ recorded at 298 – 1173 K in air

the ratio between the polymorphs A, B and C that are present in the BEA structure[23,24]. For $Mn_{4.0}SiBEA$, a small increase in intensity of the main diffraction peak at 22.50° was registered with a temperature increase from 298 to 573 K. However, at temperature higher than 573 K, a significant decrease in the intensity was observed with a simultaneous shift of the diffraction angle from 22.50° to 22.78°. Interestingly, for $Mn_{1.0}SiBEA$, during the initial stage of thermal treatment (298 – 673 K), the main diffraction peak was moved to lower Bragg angle from 22.58 to 22.52°. Presumably, this shift originated from a stronger incorporation of Mn into vacant T-atom sites of SiBEA zeolites [16,22]

Nature and environment of manganese in Mn-BEA zeolites

Diffuse reflectance UV-Vis spectroscopy

The DR UV-vis spectra of $C\text{-}Mn_{(I.E.)}AlBEA$, $C\text{-}Mn_{1.0}SiBEA$ and $C\text{-}Mn_{4.0}SiBEA$ are collected in Figure 2. For all of them the characteristic bands at 285 and 490–550 nm are seen. The first band is related to charge transfer transition between O_2-ligands and Mn(II) in the particular environment, in line with

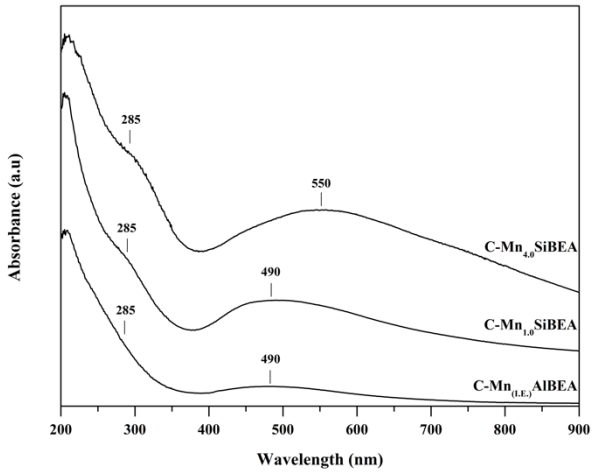

Figure 2 DR UV-Vis spectra recorded at room temperature of $C\text{-}Mn_{(I.E.)}AlBEA$, $C\text{-}Mn_{1.0}SiBEA$ and $C\text{-}Mn_{4.0}SiBEA$

other reports on Mn-containing zeolites[25,26]. The second band, observed at 490 nm for $C\text{-}Mn_{(I.E.)}AlBEA$ and $C\text{-}Mn_{1.0}SiBEA$, suggests the presence of isolated Mn(III) species in distorted tetrahedral or octahedral symmetry. In the case of $C\text{-}Mn_{4.0}SiBEA$ the maximum of the second band appeared at 550 nm due to the presence of extra-framework manganese oxide species besides framework manganese species. This observation is in line with earlier reports on Mn-containing materials[27,28].

X-ray photoelectron spectroscopy

The results of the 2p XPS characterization of $C\text{-}Mn_{(I.E.)}AlBEA$ and $C\text{-}Mn_{2.0}SiBEA$ are shown in Figure 3 and Table 1. XPS allows detection of the oxidation of Mn but it is very challenging to determine the coordination of Mn in zeolites only from XPS results. As we reported earlier, the XPS spectrum of $C\text{-}Mn_{2.0}SiBEA$ is composed of two peaks accompanied by satellite features in the $2p_{3/2}$ and $2p_{1/2}$ ranges[22]. The peaks observed at 641.5 and 653.6 eV are typical for Mn(II) species[29,30] whereas peaks at 643.3 and 655.4 eV may be ascribed to Mn(III) species[31,32] occurring in the framework in distorted tetrahedral coordination.

Table 1 XPS chemical analysis of $C\text{-}Mn_{2.0}SiBEA$ and $C\text{-}Mn_{(I.E.)}AlBEA$

Sample	Concentration (%)						Ratio
	Si 2p	O 1s	C 1s	Al 2p	Mn 2p		Mn^{III}/Mn^{II}
					Mn^{II}	Mn^{III}	
$C\text{-}Mn_{2.0}SiBEA$	31.03	53.48	15.31	-	0.11	0.06	0.61
$C\text{-}Mn_{(I.E.)}AlBEA$	29.04	55.2	14.04	1.46	0.15	0.12	0.57

The XPS spectrum of $C\text{-}Mn_{(I.E.)}AlBEA$ also consists of two peak doublets in the $2p_{3/2}$ and $2p_{1/2}$ ranges suggesting the presence

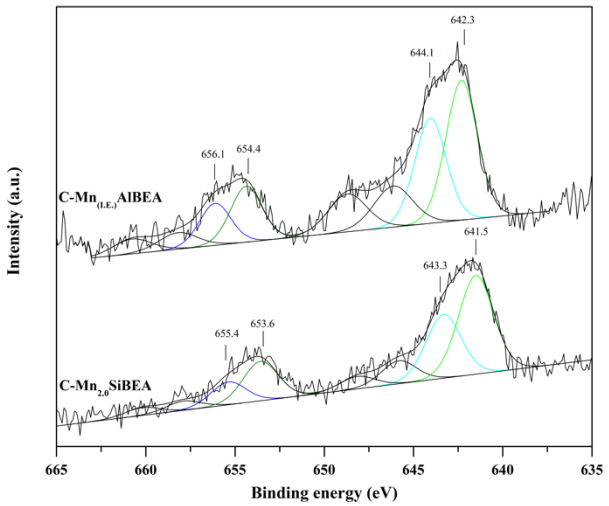

Figure 3 XPS spectra recorded at room temperature of C-$Mn_{2.0}$SiBEA and C-$Mn_{(I.E.)}$AlBEA

of Mn(II) and Mn(III) species. However, compared to the C-$Mn_{2.0}$SiBEA spectrum, the positions of the peaks are shifted to higher binding energy of ~0.8 eV. This change suggests a considerably different chemical environment of Mn in C-$Mn_{(I.E.)}$AlBEA than in C-$Mn_{2.0}$SiBEA. In the former, zeolite manganese occurs as isolated extra-framework species coordinated to framework aluminum and located in the cationic positions of BEA structure. The results of XPS chemical analysis (Table 1) revealed similar Mn(III)/Mn(II) ratio on the zeolite surface.

X-ray absorption spectroscopy

HERFD-XANES as an element specific technique was performed to characterize the local geometric and electronic structure of manganese in the studied zeolites. The HERFD-XANES spectra show sharper features and a pre-edge that is well-separated from the white line[33,34]. Figure 4 shows the spectra for calcined and rehydrated C-$Mn_{1.0}$SiBEA, C-$Mn_{2.0}$SiBEA and C-$Mn_{(I.E.)}$AlBEA. The shapes of the white lines resemble those

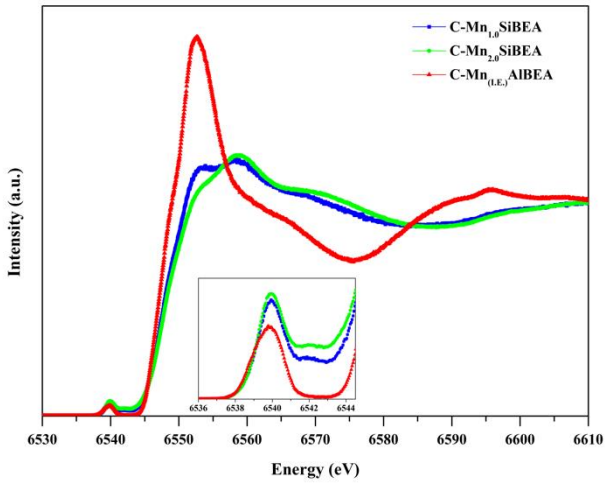

Figure 4 HERFD-XANES spectra recorded at room temperature at the Mn K edge of C-$Mn_{(I.E.)}$AlBEA, C-$Mn_{1.0}$SiBEA and C-$Mn_{2.0}$SiBEA

observed for other Mn-zeolites such as MnAPO-31[35], MnAPO-18[36] and Mn-ZSM-5[37] that contain hydrated/dehydrate, isolated Mn(II)/Mn(III) species in framework or extra-framework positions. The spectra of C-$Mn_{1.0}$SiBEA and C-$Mn_{2.0}$SiBEA are almost identical due to the uniform distribution and environment of manganese species throughout the zeolite framework. The absorption edge positions (determined as the maximum of the first derivative) for all samples are situated at around 6548 eV (differences are of 0.2 eV). With respect to the previous investigations[38] and our study on the reference samples (Fig. S1) there is a linear relation between the edges shift and the valence state of Mn for the same type of compounds (i.e. oxides)[39,40]. The shift is around 3.5 eV per oxidation degree. Thus, this parameter suggests similar valence state in all samples in contradiction to the results from other characterization techniques. Even so, the Mn K absorption main edge is strongly influenced by the local coordination, in particular inter-atomic distances[41], and is thus not necessarily a reliable indicator of the oxidation state.

The analysis of the pre-edge in the XANES spectrum may bring additional information about valence state and symmetry of the Mn species[42]. The pre-edge features may be related in a one-electron picture to electronic transition from a 1s core level to an empty orbital with strong 3d character. In line with the ligand field multiplet calculations by Radu et al.[37] and the report by Glatzel et al.[43] on the electronic structure of Mn in oxides the Mn(II) pre-edge feature in octahedral coordination has a distinct shape that arises from at two strong resonances (t_{2g} and e_g) and is placed at lower energy whereas Mn(III) has a far more complex pre-edge structure arising from the (3d,3d) electron-electron interactions. The Mn(III) spectrum shows one sharp feature at an energy similar to the Mn(II) doublet and a broad feature at about 3 eV toward higher absorption energy. The intensity of the pre-edge peaks is higher for manganese species in tetrahedral than octahedral coordination due to pd-mixing in tetrahedral symmetry[35,44]. The pre-edge of C-$Mn_{(I.E.)}$AlBEA is markedly different from that of C-$Mn_{1.0}$SiBEA and C-$Mn_{2.0}$SiBEA with lower intensity and only one feature at ca. 6539.7 eV. For C-$Mn_{1.0}$SiBEA and C-$Mn_{2.0}$SiBEA the pre-edges consist of a pronounced feature at 6539.9 eV and another peak at 6542.5 eV. Furthermore, the spectral shape resembles the one recorded for Mn_3O_4 by Glatzel et al.[43] Hence, it is probable that for C-$Mn_{1.0}$SiBEA and C-$Mn_{2.0}$SiBEA the contribution of Mn(III) is higher than in C-$Mn_{(I.E.)}$AlBEA. The higher pre-edge spectral intensity suggests the presence of Mn species in the tetrahedral and/or pseudo-tetrahedral coordination for zeolites obtained by two-step postsynthesis method. Conversely, the extra-framework species present in C-$Mn_{(I.E.)}$AlBEA are rather in octahedral coordination.

X-ray emission spectroscopy

X-ray emission spectroscopy is a very helpful tool to characterize valance states of manganese in catalytic materials[8,29,45]. We display in Figure 5 the Mn Kα XES spectra of C-$Mn_{(I.E.)}$AlBEA, C-$Mn_{1.0}$SiBEA and C-$Mn_{2.0}$SiBEA. The $K\alpha_1$ line full width at half maximum (FWHW) depends on the Mn spin multiplicity and thus oxidation and spin state. The results of

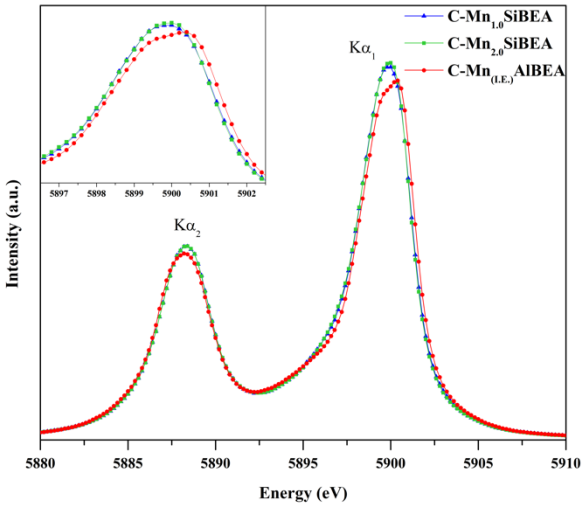

Figure 5 Mn Kα XES spectra recorded at room temperature of C-$Mn_{(I.E.)}$AlBEA, C-$Mn_{1.0}$SiBEA and C-$Mn_{2.0}$SiBEA

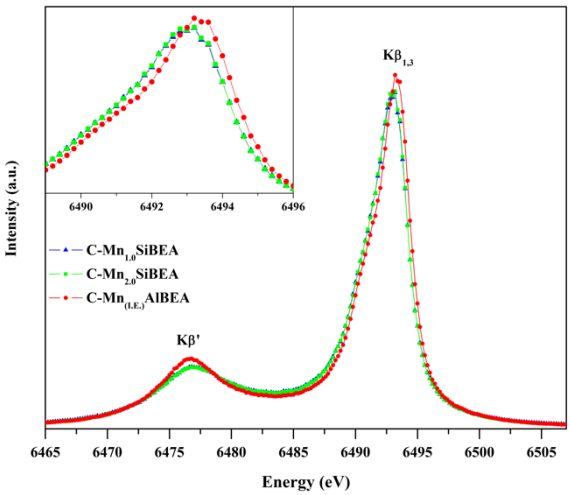

Figure 6 Mn CTC Kβ XES spectra recorded at room temperature of C-$Mn_{(I.E.)}$AlBEA, C-$Mn_{1.0}$SiBEA and C-$Mn_{2.0}$SiBEA

the XES investigation on various manganese compounds carried out by Konishi et al.[46] revealed the shift in energy and the decrease of the FWHM of Mn $Kα_1$ line with increase of the manganese valence (decrease of total spin). The XES spectra of C-$Mn_{1.0}$SiBEA and C-$Mn_{2.0}$SiBEA are almost identical with the same peak positions of $Kα_1$ at 5900 eV and values of the FWHW of 3.56 – 3.58 eV. In the case of C-$Mn_{(I.E.)}$AlBEA the $Kα_1$ line peak maximum is shifted by about 0.4 eV to higher emission energy (inset of Fig. 5) in comparison to C-$Mn_{1.0}$SiBEA and C-$Mn_{2.0}$SiBEA. In addition, the FWHW of $Kα_1$ peak is slightly wider (3.74 eV). This indicates that the Mn species in the zeolites prepared by two-step postsynthesis method may possess a higher Mn(III)/Mn(II) ratio than that of C-$Mn_{(I.E.)}$AlBEA obtained by conventional ion exchange.

We continue with the XES Kβ mainline spectra of the same samples, which are shown in Figure 6. The XES Kβ spectrum is composed of strong $Kβ_{1,3}$ peak and a broad Kβ' shoulder at lower emission energy. The splitting arises from a strong intra-atomic exchange interaction between the valence electron spin and the unpaired spin in the Mn 3p shell in the final state of the Kβ (3p to 1s) decay[47]. The manganese species with the same spin state and local environment give very similar spectra as shown for C-$Mn_{1.0}$SiBEA and C-$Mn_{2.0}$SiBEA samples. The $Kβ_{1,3}$ maximum in C-$Mn_{(I.E.)}$AlBEA at 6493.4 eV is of 0.4 eV higher than for C-Mn_xSiBEA. Simultaneously, an increase in the intensity and sharpening of the Kβ' line were observed suggesting a stronger Mn(II) character for C-$Mn_{(I.E.)}$AlBEA consistent with the observations for the Mn XES Kα lines and by HERFD-XANES. The shift of the peak maximum to the higher emitted energy indicates an increase in the total spin (reduction of oxidation degree) as we have demonstrated for a series of manganese oxides in Figure S2.

In order to complement XES study we moved our investigation to valence-to-core X-ray emission spectroscopy (vtc-XES) to probe the occupied orbitals with metal p-character a few eV below the Fermi level (valence orbitals). The vtc-XES spectrum is composed of two main features denoted as $Kβ_{2,5}$ and Kβ" and the overall spectral shape depends on the type of ligands and the local geometry. The positions and number of the main features were distinguished by fitting with Lorentzian functions as shown in Figure S4. For both C-$Mn_{1.0}$SiBEA and C-$Mn_{2.0}$SiBEA zeolites the $Kβ_{2,5}$ maxima are at 6534.8 eV whereas for C-$Mn_{(I.E.)}$AlBEA it is slightly shifted of 0.6 eV to 6534.2 eV (Fig. 7). Moreover, $Kβ_{2,5}$ of C-$Mn_{(I.E.)}$AlBEA is more intense and broader than that of C-Mn_xSiBEA. This is related to differences in the symmetry of molecular orbitals (MOs) of octahedral (O_h) and tetrahedral (T_h) complexes as Gallo et al. explained for Ti models[48]. The vtc-XES spectra of O_h complex consists of two peaks whereas T_h complex is composed of three peaks leading to broader and less intense $Kβ_{2,5}$ line as is observed for C-$Mn_{1.0}$SiBEA and C-$Mn_{2.0}$SiBEA. Bergmann et al.[49] presented earlier that the position and the intensity of the Kβ" features indicate the type of ligands and bond distances of the metal-ligand systems. They reported that an increase of the Kβ" line intensity was related to shortening of the bond between Mn and O in manganese oxide compounds. The Kβ" lines of C-$Mn_{1.0}$SiBEA and C-$Mn_{2.0}$SiBEA are at around 6520.5 – 6520.7 eV and they are equal in the intensity indicating the same type of

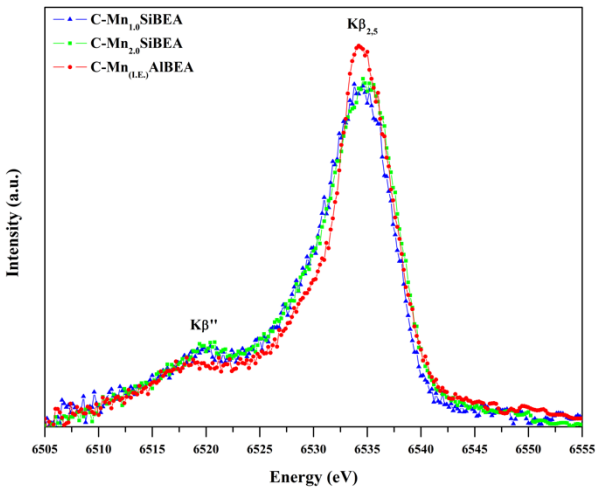

Figure 7 Mn VTC Kβ XES spectra recorded at room temperature of C-$Mn_{(I.E.)}$AlBEA, C-$Mn_{1.0}$SiBEA and C-$Mn_{2.0}$SiBEA

oxygen ligands from manganese framework species. Dissimilarly, the Kβ" of C-$Mn_{(I.E.)}$AlBEA appeared at 6518.2 eV indicating considerable different ligand environment compared to C-Mn_xSiBEA zeolites. Indeed, the manganese species occurring in the extra-framework position are coordinated with oxygen bonded to framework Al.

Thus, by combining XES and XANES investigations we can state that Mn in samples prepared by two-step postsynthesis method (C-$Mn_{1.0}$SiBEA and C-$Mn_{2.0}$SiBEA) is predominantly present as isolated species incorporated into the zeolite framework with mixed Mn(II)/Mn(III) oxidation state. On the other hand for zeolite obtained by conventional wet ion-exchange the manganese species are present in extra-framework positions mostly as Mn(II) with very small contribution of Mn(III) species.

FTIR study of manganese species and their acidity in MnSiBEA zeolites

The FTIR spectroscopy following CO sorption as a probe molecule was applied in order to study the acidic centers present in $Mn_{2.0}$SiBEA zeolites. The adsorption of CO on $Mn_{2.0}$SiBEA zeolite led to the appearance of bands at 2205, 2187, 2176, 2160 and 2140 cm^{-1} (Fig. 8A). The intensity of all bands gradually increased with successive CO doses. The two bands with highest wavenumbers at 2205 and 2187 cm^{-1} are due to interaction of CO with framework Mn(II) and Mn(III) species, respectively, most probably as a dicarbonyl moieties

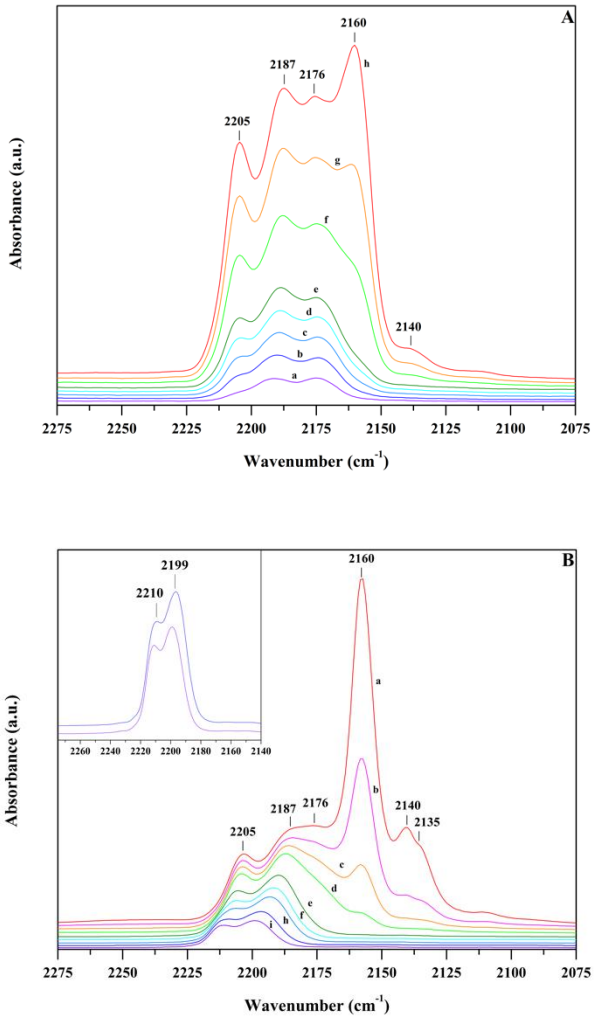

Figure 8 FTIR difference spectra recorded at 100 K in carbonyl stretching regions of $Mn_{2.0}$SiBEA (A) after adsorption of a small dose (ca. 10 μmol g^{-1} (a–d) then 45 μmol g^{-1} (e–f)) of CO and (B) evolution of the spectra in dynamic vacuum (a–g)

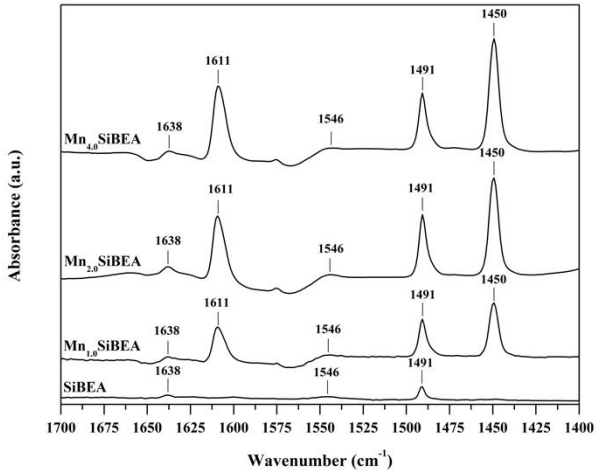

Figure 9 FTIR spectra recorded at room temperature of SiBEA, $Mn_{1.0}$SiBEA, $Mn_{2.0}$SiBEA and $Mn_{4.0}$SiBEA after adsorption of pyridine (133 Pa) for 1 h at room temperature and desorption at 423 K for 1 hour

consistent with earlier reports on Mn containing zeolite[50,51]. The band at 2176 cm^{-1} corresponds to the adsorption of CO on bridged Si–O(H)–Mn(III) groups, possess medium acidic character. Its appearance is an additional proof for the formation of isolated Mn(III) in the framework of SiBEA. The remaining band at 2161 cm^{-1} is related to silanol groups present in large quantity in $Mn_{2.0}$SiBEA in line with earlier studies of dealuminated BEA zeolite[52,53].

Table 2 Amounts of Brønsted and Lewis acidic centers in SiBEA, $Mn_{1.0}$SiBEA, $Mn_{2.0}$SiBEA and $Mn_{4.0}$SiBEA

Sample	Brønsted acidic centers (μmol g^{-1})		Lewis acidic centers (μmol g^{-1})	
	423 K	573 K	423 K	573 K
SiBEA	8	3	3	1
$Mn_{1.0}$SiBEA	22	8	74	37
$Mn_{2.0}$SiBEA	26	6	136	93
$Mn_{4.0}$SiBEA	23	9	173	103

After the introduction of CO up to 133.3 Pa (equilibrium pressure) gradual evacuation was performed as showed in Figure 8B. It can be seen that the evacuation led to complete disappearance of the bands related to physisorbed CO (2135 and 2140 cm^{-1}) and CO adsorbed on OH groups (2160 cm^{-1}). Simultaneously, for the bands at 2205 and 2187 cm^{-1} a decrease in intensity and a shift to higher wavelength were observed. The shift of the band maxima to 2210 and 2199 cm^{-1} (inset of Fig. 8B) is probably related to transformation of dicarbonyl moiety to monocarbonyl complexes Mn(II)–(CO) and Mn(III)–(CO), respectively[54,55]. The fact that these two bands are seen in the FTIR spectrum even after profound evacuation proves the high stability of bonds between

manganese and carbon monoxides and their strong acidic character.

The FTIR investigation combined with pyridine sorption may reveal not only the number of acidic sites but also their strength and various natures. The difference spectra of pyridine adsorbed on SiBEA, $Mn_{1.0}$SiBEA, $Mn_{2.0}$SiBEA and $Mn_{4.0}$SiBEA are shown in Figure 9. With respect to SiBEA very low intense bands at 1638, 1546, and 1491 cm^{-1} are observed, illustrating low concentration of Brønsted and Lewis acidic sites (Table 2)[56,57]. The introduction of manganese in SiBEA resulted in increasing the band at 1450 cm^{-1} suggesting the formation of new Lewis acidic sites in Mn_xSiBEA due to the existence of framework mononuclear Mn species. Furthermore, in the FTIR spectra of $Mn_{1.0}$SiBEA, $Mn_{2.0}$SiBEA and $Mn_{4.0}$SiBEA the intensity of the bands at 1546 and 1638 cm^{-1} increased suggesting the formation of an additional amount of Brønsted acidic sites probably due to the presence of bridging hydroxyl groups Si–O(H)–$Mn^{(III)}$. Similar observations were reported for FeSiBEA zeolites by Hnat et al. [58]

Catalytic results

Figure 10 exhibits the NO conversion in NH_3-SCR on $Mn_{1.0}$SiBEA, $Mn_{2.0}$SiBEA, $Mn_{4.0}$SiBEA and $Mn_{(I.E.)}$AlBEA zeolite catalysts. The huge difference in DeNO$_x$ activity between two types of catalysts is clearly seen. The catalysts obtained with two-step postsynthesis method showed high activity at low and medium temperature range while the catalyst obtained by conventional wet ion exchange performed poor activity in the 423 – 623 K range. Nevertheless, differences in catalytic activity were also seen between $Mn_{1.0}$SiBEA, $Mn_{2.0}$SiBEA and $Mn_{4.0}$SiBEA. In the low temperature range (423 – 523 K) the NO conversion increased with increasing reaction temperature reaching maximum conversion of 96 % for $Mn_{4.0}$SiBEA and only slightly lower for $Mn_{2.0}$SiBEA and $Mn_{1.0}$SiBEA, 93 and 89 % respectively. In the medium temperature range (523 K – 623 K)

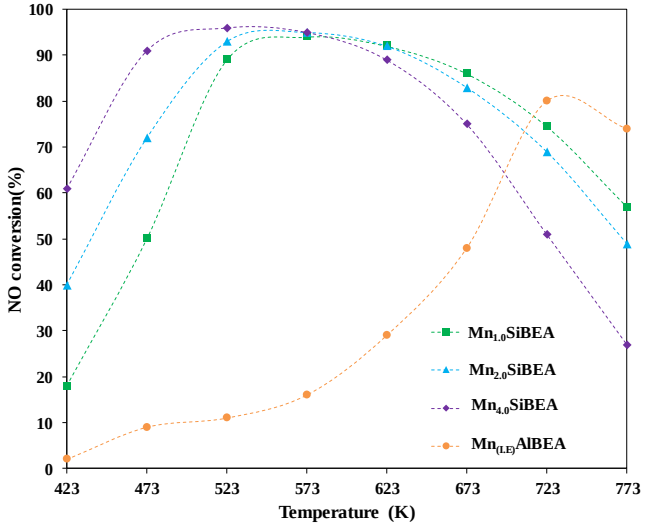

Figure 10 NO conversion in SCR of NO with NH_3 on $Mn_{1.0}$SiBEA, $Mn_{2.0}$SiBEA, $Mn_{4.0}$SiBEA and $Mn_{(I.E.)}$AlBEA

the activity of all three catalysts remained high with NO conversion of 96 – 89 %. It is well known that manganese containing materials are highly effective in SCR process at low temperature[7,11]. The catalysts described in the literature were often doped with high Mn loading leading to the formation of surface manganese oxides (MnO_2 and Mn_3O_4) which were responsible for excellent activity. While the reaction temperature increases, a sharp drop in catalytic activity was observed. The proposed reason for this was the ammonia oxidation to N_2O, which is accelerated by large MnO_x clusters at elevated temperature. The analysis of the selectivity of the catalysts (Fig. 11) revealed that the application of all samples resulted in very high N_2 selectivity (~100 %) at 423 – 573 K. Even though, gradual decrease in selectivity toward N_2 was

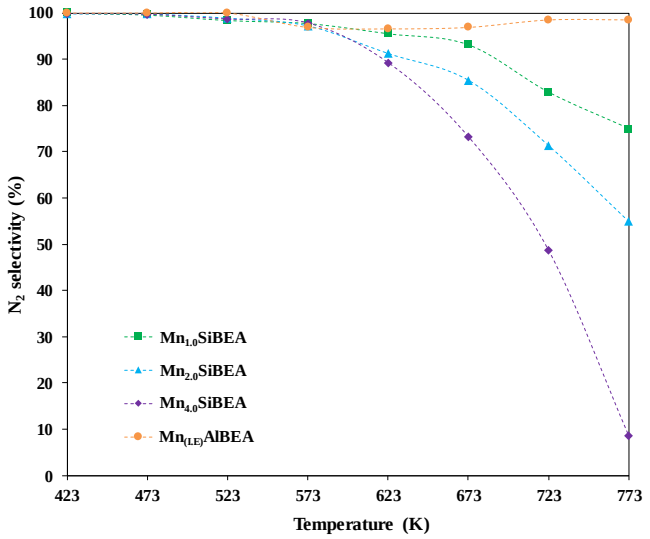

Figure 11 N_2 selectivity in SCR of NO with NH_3 on $Mn_{1.0}$SiBEA, $Mn_{2.0}$SiBEA, $Mn_{4.0}$SiBEA and $Mn_{(I.E.)}$AlBEA

observed over 573 K for Mn_xSiBEA catalysts depending on Mn concentration. Significant loss in N_2 yield appeared in particular for $Mn_{4.0}$SiBEA whereas for $Mn_{1.0}$SiBEA the decrease was much smaller. Conversely, in case of $Mn_{(I.E.)}$AlBEA the N_2 selectivity remained high and stable over the whole studied temperature range. Furthermore, for this catalyst output in NO removal strongly increased at 723 – 773 K reaching 80% in NO conversion, the highest value among all tested samples.

The decrease in catalyst efficiency was strongly correlated with the type of manganese species occurring in zeolites and with N_2O formation. The polynuclear extra-framework species present in $Mn_{4.0}$SiBEA were responsible for high NO conversion at low temperature but at high temperature led predominantly to oxidation of ammonia to N_2O. For $Mn_{1.0}$SiBEA the formation of N_2O seems to be a minor problem and for $Mn_{(I.E.)}$AlBEA it is almost negligible. The catalytic results show that valence state and environment of manganese species have strong impact on the activity in SCR of NO. The mononuclear, framework Mn species present in $Mn_{1.0}$SiBEA and $Mn_{2.0}$SiBEA as Mn(II) and Mn(III) allowed obtaining high NO conversion and N_2 selectivity in the 573 – 723 K range. Despite poor performance at 423 – 623 K, the $Mn_{(I.E.)}$AlBEA

catalyst gave unexpectedly high activity at 723 – 773 K. Probably, the vicinity of Al species improved the catalytic activity of isolated, extra-framework manganese and prevented the N_2O formation. The acidic sites present in this type of catalysts may also play an important role in the catalytic mechanism according to our previous report[19].

Conclusions

The modifications of zeolite beta by two different postsynthesis preparation methods led to two types of catalysts with considerably different manganese species. In the zeolites obtained by two-step postsynthesis method, with low metal content (up to 2 wt %), manganese is present in the framework positions as Mn(II) and Mn(III) species. In the C-$Mn_{(I.E.)}$AlBEA zeolite, prepared with conventional wet ion exchange method, manganese was predominantly present as extra-framework octahedral Mn(II) species. Both groups of zeolites possess high thermal stability as evidenced by HT-XRD. $Mn_{1.0}$SiBEA and $Mn_{2.0}$SiBEA catalysts showed significant activity in the SCR process with NO conversion of about 89 – 96 % and high N_2 selectivity in the medium temperature range. The drop of ca. 20 % in selectivity toward N_2 at 723 – 773 K range seemed to be due to N_2O formation. On the other hand, $Mn_{(I.E.)}$AlBEA showed excellent selectivity to the desired product in the whole temperature range but it gave high NO conversion only at elevated temperature. Thus, it was shown that the location of manganese species, their state as well as the acidity played an important role in NH_3-SCR.

Acknowledgements

Part of this project was funded by the National Science Centre Poland (NCN) on the basis of the decision number UMO-2012/07/N/ST5/00171 – "PRELUDIUM" grant (R.B., S.D.). Teresa Grzybek would like to acknowledge for the financial support of AGH grant: 11.11.210.213.

Notes and references

1 L. Kubiak, R. Matarrese, L. Castoldi, L. Lietti, M. Daturi and P. Forzatti, *Catalysts*, 2016, **6**, 36–52.
2 R. Baran, T. Grzybek, T. Onfroy and S. Dzwigaj, *Micropor. Mesopor. Mater.*, 2016, **226**, 104–109.
3 D. Wierzbicki, R. Dębek, J. Szczurowski, S. Basąg, M. Włodarczyk, M. Motak and R. Baran, *Comptes Rendus Chim.*, 2015, **18**, 1074–1083.
4 L. Castoldi, R. Bonzi, L. Lietti, P. Forzatti, S. Morandi, G. Ghiotti and S. Dzwigaj, *J. Catal.*, 2011, **282**, 128–144.
5 J. Szanyi, J. H. Kwak, H. Zhu and C. H. F. Peden, *Phys. Chem. Chem. Phys.*, 2013, **15**, 2368–2380.
6 A. Sultana, M. Sasaki and H. Hamada, *Catal. Today*, 2012, **185**, 284–289.
7 G. Qi, R. T. Yang and R. Chang, *Catal. Letters*, 2003, **87**, 67–71.
8 G. Lv, F. Bin, C. Song, K. Wang and J. Song, *Fuel*, 2013, **107**, 217–224.
9 M. Kang, E. D. Park, J. M. Kim and J. E. Yie, *Appl. Catal. A Gen.*, 2007, **327**, 261–269.
10 P. R. Ettireddy, N. Ettireddy, S. Mamedov, P. Boolchand and P. G. Smirniotis, *Appl. Catal. B*, 2007, **76**, 123–134.
11 F. Liu, H. He, Y. Ding and C. Zhang, *Appl. Catal. B*, 2009, **93**, 194–204.
12 X. Liang, J. Li, Q. Lin and K. Sun, *Catal. Commun.*, 2007, **8**, 1901–1904.
13 B. Samojeden, M. Motak and T. Grzybek, *Comptes Rendus Chim.*, 2015, **18**, 1049–1073.
14 J. Y. Favez, M. Weilenmann and J. Stilli, *Atmos. Environ.*, 2009, **43**, 996–1007.
15 E. Borfecchia, K. A. Lomachenko, F. Giordanino, H. Falsig, P. Beato, A. V. Soldatov, S. Bordiga and C. Lamberti, *Chem. Sci.*, 2015, **6**, 548–563.
16 S. Dzwigaj, P. Massiani, A. Davidson and M. Che, *J. Mol. Catal. A Chem.*, 2000, **155**, 169–182.
17 S. Dzwigaj, M. Matsuoka, R. Franck, M. Anpo and M. Che, *J. Phys. Chem. B*, 1998, **102**, 6309–6312.
18 R. Baran, Y. Millot, T. Onfroy, J. M. Krafft and S. Dzwigaj, *Micropor. Mesopor. Mater.*, 2012, **163**, 122–130.
19 R. Baran, F. Averseng, D. Wierzbicki, K. Chalupka, J. M. Krafft, T. Grzybek and S. Dzwigaj, *Appl. Catal. A*, 2016, **523**, 332–342.
20 R. Baran, T. Onfroy, S. Casale and S. Dzwigaj, *J. Phys. Chem. C*, 2014, **118**, 20445–20451.
21 E. Gallo and P. Glatzel, *Adv. Mater.*, 2014, **26**, 7730–7746.
22 R. Baran, L. Valentin and S. Dzwigaj, *Phys. Chem. Chem. Phys.*, 2016, **18**, 12050–12057.
23 J. B. Higgins, R. B. LaPierre, J. L. Schlenker, A. C. Rohrman, J. D. Wood, G. T. Kerr and W. J. Rohrbaugh, *Zeolites*, 1988, **8**, 446–452.
24 M. M. J. Treacy and J. M. Newsam, *Nature*, 1988, 332, 249–251.
25 S. N. Azizi and S. Ehsani Tilami, *J. Solid State Chem.*, 2013, **198**, 138–142.
26 B. Qi, X. H. Lu, D. Zhou, Q. H. Xia, Z. R. Tang, S. Y. Fang, T. Pang and Y. L. Dong, *J. Mol. Catal. A Chem.*, 2010, **322**, 73–79.
27 T. Kharlamova, G. Mamontov, M. Salaev, V. Zaikovskii, G. Popova, V. Sobolev, A. Knyazev and O. Vodyankina, *Appl. Catal. A*, 2013, **467**, 519–529.
28 V. Mahdavi and M. Mardani, *Mater. Chem. Phys.*, 2015, **155**, 136–146.
29 Q. Lin, J. Li, L. Ma and J. Hao, *Catal. Today*, 2010, **151**, 251–256.
30 M. Stanciulescu, G. Caravaggio, A. Dobri, J. Moir, R. Burich, J.-P. Charland and P. Bulsink, *Appl. Catal. B*, 2012, **123–124**, 229–240.
31 H. Pan, Q. Su, J. Chen, Q. Ye, Y. Liu and Y. Shi, *Environ. Sci. Technol.*, 2009, **43**, 9348–9353.
32 X. Zhang, B. Shen, K. Wang and J. Chen, *J. Ind. Eng. Chem.*, 2013, **19**, 1272–1279.
33 S. Lafuerza, J. Garcia, G. Subias, J. Blasco and P. Glatzel, *Phys. Rev. B*, 2016, **93**, 205108-1-205108–11.
34 P. Glatzel, F. M. F. De Groot, O. Manoilova, D. Grandjean,

B. M. Weckhuysen, U. Bergmann and R. Barrea, *Phys. Rev. B*, 2005, **72**, 14117-1-14117–7.
35 N. Novak Tusar, G. Mali, I. Arcon, V. Kaučič, A. Ghanbari-Siahkali and J. Dwyer, *Micropor. Mesopor. Mater.*, 2002, **55**, 203–216.
36 F. Corà, G. Sankar, C. R. A. Catlow and J. M. Thomas, *Chem. Commun.*, 2002, **21**, 734–735.
37 D. Radu, P. Glatzel, A. Gloter, O. Stephan, B. M. Weckhuysen and F. M. F. De Groot, *J. Phys. Chem. C*, 2008, **112**, 12409–12416.
38 I. Arcon, N. Novak Tusar, A. Ristic, A. Kodre and V. Kaučič, *Phys. Scr.*, 2005, **T115**, 810–812.
39 S. J. A. Figueroa, F. G. Requejo, E. J. Lede, L. Lamaita, M. A. Peluso and J. E. Sambeth, *Catal. Today*, 2005, **107–108**, 849–855.
40 F. H. B. Lima, M. L. Calegaro and E. A. Ticianelli, *J. Electroanal. Chem.*, 2006, **590**, 152–160.
41 P. Glatzel, G. Smolentsev and G. Bunker, *J. Phys. Conf. Ser.*, 2009, **190**, 12046.
42 V. Cuartero, S. Lafuerza, M. Rovezzi, J. García, J. Blasco, G. Subías and E. Jiménez, *Phys. Rev. B*, 2016, **94**, 155117-1-155117–10.
43 P. Glatzel, U. Bergmann, J. Yano, H. Visser, J. H. Robblee, W. Gu, F. M. F. De Groot, G. Christou, V. L. Pecoraro, S. P. Cramer and V. K. Yachandra, *J. Am. Chem. Soc.*, 2004, **126**, 9946–9959.
44 F. Farges, *Phys. Rev. B*, 2005, **71**, 155109-1-155109–14.
45 X. Tang, J. Fei, Z. Hou, X. Zheng and H. Lou, *Energy & Fuels*, 2008, **22**, 2877–2884.
46 T. Konishi, T. Tsubata, M. Oku, Y. M. Todorov and M. Yoshio, *Anal. Sci.*, 2005, **21**, 861–864.
47 M. Rovezzi and P. Glatzel, *Semicond. Sci. Technol.*, 2014, **29**, 1–19.
48 E. Gallo, F. Bonino, J. C. Swarbrick, T. Petrenko, C. Lamberti and P. Glatzel, *ChemPhysChem Commun.*, 2013, **14**, 79–83.
49 U. Bergmann, C. R. Horne, T. J. Collins, J. M. Workman and S. P. Cramer, *Chem. Phys. Lett.*, 1999, **302**, 119–124.
50 D. B. Akolekar and S. K. Bhargava, *Appl. Catal. A*, 2001, **207**, 355–365.
51 K. Hadjiivanov, E. Ivanova, M. Kantcheva, E. Z. Ciftlikli, D. Klissurski, L. Dimitrov and H. Knözinger, *Catal. Commun.*, 2002, **3**, 313–319.
52 K. Hadjiivanov, A. Penkova, R. Kefirov, S. Dzwigaj and M. Che, *Micropor. Mesopor. Mater.*, 2009, **124**, 59–69.
53 R. Kefirov, E. Ivanova, K. Hadjiivanov, S. Dzwigaj and M. Che, *Catal. Letters*, 2008, **125**, 209–214.
54 K. I. Hadjiivanov and G. N. Vayssilov, *Adv. Catal.*, 2002, **47**, 307–511.
55 M. C. Campa, D. Pietrogiacomi, S. Tuti, G. Ferraris and V. Indovina, *Appl. Catal. B Environ.*, 1998, **18**, 151–162.
56 M. Trejda, M. Ziolek, Y. Millot, K. Chalupka, M. Che and S. Dzwigaj, *J. Catal.*, 2011, **281**, 169–176.
57 J. N. Kondo, R. Nishitani, E. Yoda, T. Yokoi, T. Tatsumi and K. Domen, *Phys. Chem. Chem. Phys.*, 2010, **12**, 11576–11586.
58 I. Hnat, I. Kocemba, J. Rynkowski, T. Onfroy and S. Dzwigaj, *Catal. Today*, 2011, **176**, 229–233.